

See discussions, stats, and author profiles for this publication at: <https://www.researchgate.net/publication/46179688>

# Molecular Behavior of DNA Origami in Higher-Order Self-Assembly

ARTICLE *in* JOURNAL OF THE AMERICAN CHEMICAL SOCIETY · SEPTEMBER 2010

Impact Factor: 12.11 · DOI: 10.1021/ja106292x · Source: PubMed

CITATIONS

50

READS

37

6 AUTHORS, INCLUDING:



Zhe li

Arizona State University

11 PUBLICATIONS 260 CITATIONS

SEE PROFILE



Minghui Liu

Arizona State University

12 PUBLICATIONS 628 CITATIONS

SEE PROFILE



Hao Yan

National Cheng Kung University

28 PUBLICATIONS 937 CITATIONS

SEE PROFILE



Yan Liu

Arizona State University

151 PUBLICATIONS 6,815 CITATIONS

SEE PROFILE

Published in final edited form as:

*J Am Chem Soc.* 2010 September 29; 132(38): 13545–13552. doi:10.1021/ja106292x.

## Molecular Behavior of DNA Origami in Higher-Order Self-Assembly

Zhe Li<sup>†</sup>, Minghui Liu<sup>†</sup>, Lei Wang<sup>†,‡</sup>, Jeanette Nangreave<sup>†</sup>, Hao Yan<sup>†</sup>, and Yan Liu<sup>\*,†</sup>

Department of Chemistry and Biochemistry and The Biodesign Institute, Arizona State University, Tempe, Arizona 85287, and School of Pharmaceutical Sciences, Shandong University, Jinan 250012, P. R. China

### Abstract

DNA-based self-assembly is a unique method for achieving higher-order molecular architectures made possible by the fact that DNA is a programmable information-coding polymer. In the past decade, two main types of DNA nanostructures have been developed: branch-shaped DNA tiles with small dimensions (commonly up to ~20 nm) and DNA origami tiles with larger dimensions (up to ~100 nm). Here we aimed to determine the important factors involved in the assembly of DNA origami superstructures. We constructed a new series of rectangular-shaped DNA origami tiles in which parallel DNA helices are arranged in a zigzag pattern when viewed along the DNA helical axis, a design conceived in order to relax an intrinsic global twist found in the original planar, rectangular origami tiles. Self-associating zigzag tiles were found to form linear arrays in both diagonal directions, while planar tiles showed significant growth in only one direction. Although the series of zigzag tiles were designed to promote two-dimensional array formation, one-dimensional linear arrays and tubular structures were observed instead. We discovered that the dimensional aspect ratio of the origami unit tiles and intertile connection design play important roles in determining the final products, as revealed by atomic force microscopy imaging. This study provides insight into the formation of higher-order structures from self-assembling DNA origami tiles, revealing their unique behavior in comparison with conventional DNA tiles having smaller dimensions.

### Introduction

DNA self-assembly has shown great promise for the construction of nanoscale architectures. A large variety of one-, two-, and even three-dimensional (1D, 2D, and 3D) DNA nanostructures<sup>1–27</sup> have been successfully assembled using branched motifs (tiles) as the basic structural units, and these nanostructures have been used to precisely organize a variety of functional materials.<sup>28–39</sup> Among the many exciting achievements, scaffolded DNA origami is especially remarkable for its capacity to yield complex and fully addressable patterns. In this method, a long single strand of DNA (e.g., 7.2 kb genome of phage M13mp18) is folded into 2D or 3D<sup>40–48</sup> structures by hundreds of short complementary DNA strands (staples). Each staple strand occupies a specific position as a result of its unique sequence complementary to the genomic DNA strand; thus, DNA origami tiles exhibit fully addressable surfaces that can be used to organize proteins,

© 2010 American Chemical Society

<sup>†</sup>Arizona State University.

<sup>‡</sup>Shandong University.

Supporting Information Available: DNA sequences, materials, methods, and additional AFM results. This material is available free of charge via the Internet at <http://pubs.acs.org>.

nanoparticles, or carbon nanotubes and carry out single-molecule chemical reactions with spatial control.<sup>34,49–57</sup>

One of the central goals in nanotechnology is to assemble unit building blocks into higher-order periodic or nonperiodic architectures. With the proper sticky end design, individual DNA origami tiles can act as basic structural units and self-assemble into larger 1D, 2D, and 3D structures. However, reports of large arrays formed from DNA origami tiles have been quite limited. In one example, Rothemund demonstrated that triangular-shaped DNA origami tiles can be connected through stable strand linkages to form fixed-size 2D arrays, although the size and yield of the arrays was quite small.<sup>40</sup> In another study, rectangular-shaped DNA origami tiles originally designed by Rothemund were successfully used to construct 1D arrays,<sup>58</sup> but efforts to make 2D arrays with dimensions larger than 1  $\mu\text{m}$  using these rectangular tiles have proven to be difficult (see the Supporting Information). Collectively, these observations suggest that DNA origami, with its large dimensions and unique characteristics, behaves somewhat differently from small DNA tiles. It is worth pointing out that the systematic study of the higher-order self-assembly of small DNA tiles has been performed by various groups, and abundant information has been gathered<sup>15,16,20,37</sup> that has led to greater control over product assembly. In contrast, the study of the higher-order assembly of large DNA origami tiles is lacking. Can the knowledge gained from small tiles be directly applied to large origami tiles when creating higher-order superstructures? This work aimed to address this critical question in a systematic way and to determine the important factors involved in the assembly of DNA origami tiles into higher-order superstructures.

In an attempt to establish the significant structural properties of origami tiles, a close examination of Rothemund's original design for rectangular-shaped DNA origami tiles was carried out. One important aspect of the original design relates to the crossovers between parallel helices: periodic crossovers are separated by odd numbers of half-turns, with 16 base pairs (bp) considered as 1.5 turns. This results in a twist density of 10.67 bp per turn (16 bp/1.5 turns), which represents a slight underwinding of all of the DNA helices relative to the 10.5 bp per turn in B-form DNA. Since there are over 200 crossovers in a single tile structure, the local underwinding per helical turn may lead to a considerable global twist deformation, preventing the formation of planar 2D lattice superstructures.

Here we present a new design for the rectangular-shaped DNA origami that is intended to relieve the deformation; it contains dihedral angles of  $120^\circ$  when viewed along the helical axes (Figure 1A,B) and is hereafter called “zigzag DNA origami”. The number of base pairs between consecutive crossovers of neighboring helices alternates between 14 bp and 28 bp (Figure 1C), corresponding to exactly  $4/3$  or  $8/3$  turns, respectively:<sup>18,20,43</sup> 14 bp is equal to one full turn plus  $120^\circ$ , and 28 bp is two full turns plus  $240^\circ$ . Thus, two adjacent crossovers within the same helix are spaced exactly four turns apart. The twist density of this design is 10.5 bp per turn,<sup>20</sup> the same as in B-form DNA, so the global twisting of the structure should be minimized.

Figure 1C illustrates the folding path of a zigzag origami, in which a 7056 nucleotide (nt) strand of M13mp18 (black) was folded into a rectangular structure using 168 staples (blue), with individual staples spanning three helices and containing either  $7n$  or  $14n$  ( $n = 3, 4, \text{ or } 5$ ) nucleotides. The remaining nucleotides of the scaffold strand were left as an unpaired loop bridging the starting and ending points of the folding path. The length of the DNA origami tile in the direction parallel to the helical axis (the  $x$  direction) was  $\sim 100$  nm. In the  $y$  direction, with an assumed interhelical distance of 0.5 nm,<sup>40</sup> the 24 parallel helices should have formed a corrugated structure with a length of  $\sim 52$  nm. However, once the origami tile was deposited on a mica substrate and scanned using atomic force microscopy (AFM) in

tapping mode, the dimensions of the origami tiles were measured to be  $\sim 100 \text{ nm} \times 60 \text{ nm}$ . The stretching in the  $y$  direction may have been due to attractive interactions with the hydrophilic mica surface, where the DNA tiles were presumably flattened to maximize contact.

## Results and Discussion

### Assembly of Stairlike 1D Arrays

First, the planar and zigzag DNA origami tiles were designed to self-associate through linker strands bridging diagonal corners and assemble into stairlike linear arrays. Figure 2A illustrates the assembly strategy. For both types of origami tiles, the core structures (with the far left and right columns of staples omitted) were first assembled following a standard origami annealing protocol (see the Supporting Information for details). Unpaired regions of M13 in the four corners of the tiles are numbered as 1, 2, 3, and 4, each spanning 12 helices. Two sets of 12 linker strands were deliberately designed, one to link corner 1 to corner 3 and the other to link corner 2 to corner 4. The individual linker strands consisted of two binding domains: one containing a sequence complementary to the unpaired region of M13 in one corner and the second containing a sequence complementary to the unpaired region of M13 in the opposite diagonal corner. When the “1–3” set of strands were added to the preannealed origami cores and incubated at room temperature overnight, the result was a stairlike array connected in the 1–3 direction. Similarly, the “2–4” linkers were used to connect the preannealed origami cores in the other diagonal direction.

AFM imaging of the final structures revealed that employing 1–3 connections resulted in stairlike 1D arrays with a maximum length of  $\sim 40$  tiles for both the zigzag origami (Figure 2C) and the planar origami (Figure 2F). In contrast, the 1D arrays formed from zigzag and planar origami connected through corners 2 and 4 were distinct. The zigzag origami assembled into long, linear arrays similar to those formed through 1–3 connections (Figure 2D), while the planar origami assembled into twisted (right-handed) helical superstructures (Figure 2G) with every other tile forming a half-twist (see the inset of Figure 2G). This observation supports our assumption that planar DNA origami does not adopt a perfectly flat arrangement but instead displays a global pucker. This also indicates that the bending of the tile is severe in the 2–4 diagonal direction but minimal in the 1–3 diagonal direction. The observation of a right-handed twist agrees with the results reported by Shih's group,<sup>43</sup> in which an origami structure with a helical twist density of greater than 10.5 bp per turn was used. It should be pointed out that the long linear arrays formed by the zigzag origami in the 2–4 direction also displayed some degree of twisting at certain sites (Figure 2D) but with a much lower frequency. A side-by-side comparison of these two designs indicated that the zigzag origami did not experience as much structural strain as the planar origami, with less twisting and bending out of the plane; therefore, the zigzag origami tile was presumed to be more suitable to serve as a basic structural unit for higher-order assembly purposes and was utilized for all subsequent assembly experiments.

### Formation of DNA Origami Tubes

Experiments were conducted in which both sets of linker strands (for 1–3 connections and 2–4 connections) were added to preformed zigzag core structures, and rather than the expected 2D lattices, the formation of tubes was observed. The tubes were assembled by two independent methods: by either combining all 24 linkers simultaneously with the core structures or using a stepwise assembly approach. For the stepwise method, stairlike arrays were first formed in one direction using one set of linkers, after which the second set of linkers was added. The two methods yielded similar tube structures, as shown in Figure 3A, with most of the tubes having lengths of 1–3  $\mu\text{m}$ . Individual origami tiles are clearly visible

in the zoom-in insets in Figure 3A, with the observed length in agreement with the expected 100 nm. The profile of a cross section of a single tube (Figure 3B) shows that the tube was 3 nm in height (double the height of an individual origami tile) and ~30 nm in width (about half the width).

Figure 3C illustrates one possible mechanism for the formation of the observed tube structures. One set of linkers first recognizes the corresponding complementary regions of the origami core structures, initially connecting several origami tiles into a stairlike ribbon; similarly, recognition by the other set of linkers forms a stairlike ribbon with the opposite connectivity. Once they are assembled into a stairlike ribbon, it is then presumably faster and easier for the linkers that are not involved in intertile connections to bind to M13 in an adjacent tile within the same ribbon rather than in a different ribbon, which would require travel over a much greater distance considering the low concentration (nM). Formation of a tube may also be thermodynamically preferred because tube closure is the most efficient process to minimize the number of unpaired DNA strands. Because of the intrinsic flexibility of the origami tiles (resulting from the numerous nick points within the structure), bending of the origami tile in both the *x* and *y* directions is possible. Apparently, the preferred bending path for the 24-helix tiles is in the *y* direction, which might be a result of the shorter distance the linkers must traverse to form a closed structure. This interaction rolls the connected ribbon into a tube whose axis is parallel to the helical axis of the tiles and whose circumference is equal to the width of a single tile. Additionally, the tubes are not completely sealed, as there is no linkage between the top and bottom edges of each origami tile; thus, they are readily opened by AFM imaging, providing further evidence of tube morphology.

For comparison, surface-mediated assembly of origami core structures together with all 24 linkers was also performed.<sup>59</sup> Rather than the formation of tubes as seen in the solution-based assembly, the formation of small pieces (~10 tiles) of 2D arrays was observed because the solid support provided many nucleation points (see the Supporting Information for details). The attractive interactions between the origami tiles and the flat, hydrophilic solid support must restrict the bending of the tiles and render them inflexible, causing the intertile interaction to dominate and ultimately lead to the formation of 2D lattices. However, the size of the 2D lattices obtained using this method showed no improvement over those in existing reports. The relatively low efficiency of the surface-mediated self-assembly of origami tiles relative to that of small DNA tiles or short DNA strands could be due to the low concentration (nM vs  $\mu$ M) and the large unit size of the origami tiles, which results in reduced lateral mobility on the mica surface.

### **Tailoring the Structural Features of Origami Tubes by Varying the Dimensions and Intertile Connections of the Zigzag Tile Units**

On the basis of the proposed tube formation mechanism, several structural factors could be varied to manipulate the assembly process and obtain unique products. We hypothesized that the number and position of the linker strands would control the morphology of the final structures. In addition, we presumed that tiles with varying dimensional aspect ratios would also generate unique tube structures.

We first examined how varying the number of linkers between tiles would impact the final structures. A gap between corners 1 and 4 and corners 2 and 3 of the origami tile is formed when less than 24 linkers are used, and a smaller number of linkers between tiles produces a wider gap, as illustrated in the schemes in Figure 4. Upon addition of 20 linkers (10 strands from each set) to the preformed zigzag core structures, formation of origami tubes with the expected four-helix gap (~6.5 nm) was observed (Figure 4A). The zoom-in image shows alternating single-layer and double-layer regions, confirming the existence of the gaps, as

schematically illustrated in Figure 4A. Similarly, tubes were also observed when 16 linkers were used (Figure 4B). However, when the number of linker strands was reduced to 12 or 8, 1D origami chains rather than tubes were observed (Figure 4C,D, respectively). It may be that when the number of linker strands is decreased this much, the free energy that is gained through intertile bond associations is not enough to pay the energy penalty for bending of the origami tiles into tubes. In this case, a half-turn twist in the linker region between two neighboring tiles yields a planar structure, as shown in Figure 4C,D. It is also possible that tubular structures actually form but that the wide gap makes the tubes susceptible to deformation, causing them to collapse when they are deposited onto the mica before imaging can confirm their existence.

To investigate the effect of the tile dimensions on the superstructure assembly, we first designed a zigzag origami tile containing 12 parallel helices that had dimensions of  $200 \text{ nm} \times 26 \text{ nm}$  (Figure 5A). In comparison with the 24-helix zigzag origami, the new design was twice as long in the  $x$  direction and half as wide in the  $y$  direction. After the assembly of the core structures, 12 linkers (six strands of each set) were added to the solution to link diagonal corners of the tiles following the same design strategy as for the 24-helix tiles. However, rather than 2D arrays or tubes, only 1D chains were observed by AFM (Figure 5B). The decreased width of the origami tile significantly increases the energy required to bend the tile in the  $y$  direction, making it harder to roll the tile into a tube. It is intriguing to notice that bright spots between adjacent tiles are clearly visible along the chain, corresponding to an increase in height from 1.5 nm (single-layer origami tiles) to  $\sim 3 \text{ nm}$  at these connection points. On the basis of this observation, we illustrate the possible formation mechanism in Figure 5C. For kinetic reasons, the linkers may prefer to bind to complementary regions within the same chain by attaching to the next tile end-to-end rather than binding to a third tile. The linker strands appear to cross in the center between two neighboring tiles, though an energy penalty for bending of the helices of the linker strands in the plane of the tile is required. The overlap of the linkers at the connection points between neighboring tiles forms the high spots observed by AFM.

To further test the effect of varying the dimensional aspect ratio, we designed a third version of the zigzag origami tile containing 40 helices (Figure 6A) with dimensions of  $\sim 57 \text{ nm} \times 86 \text{ nm}$ , which is shorter in the  $x$  direction and wider in the  $y$  direction than the 24-helix tile. The dominant structures that were formed when all 40 linker strands were added to the core structure were ribbons with periodic one- and two-layer height changes (Figure 6B). In addition, a small fraction of linear, double-layered ribbons having a width equal to the  $x$  dimension of the unit tile were observed (Figure 6C).

The proposed mechanisms of formation of these two ribbon products are shown in Figure 6D. The initial assembly is very similar to that of the 24-helix origami in which one set of linkers recognizes the complementary regions in the origami core structures, yielding a staggered ribbon. However, rather than bending the tiles in the  $y$  direction in the same manner as the 24-helix tile, the subsequent binding of the second set of linkers results in two other types of connections. In the first case, the origami tiles bend, with sticky ends within the same tile binding at diagonal corners, resulting in the double-layer regions observed in the ribbon. In this way, all of the sticky ends travel the shortest distance to bind to complementary regions of the core, but this requires overcoming the energy barrier for bending and twisting of the origami tile. In the second case, linear double-layer ribbons (or tubes) with a circumference equal to twice the width of the tile that grow in the  $y$  direction are observed. We observed far fewer double-layer linear ribbons than twisted ribbons, which is likely a result of the greater bending energy required for the parallel helices to bend out of the plane of the tile.



## Summary and Discussion

We have designed and characterized a new family of rectangular-shaped DNA origami tiles in which the global twist found in typical “planar” origami has been relaxed, yielding a structural unit with the potential to self-assemble into larger and more complex nanostructures. When a linker-strand connection strategy was used, the formation of either tubular structures or 1D arrays was observed (Figure 7), depending on the dimensional aspect ratio of the origami DNA tiles and the number of linker strands utilized. Our observations indicate that the higher-order assembly process for origami tiles (~7000 bp per tile) is markedly different from that for small DNA tiles (80–400 bp per tile), although it follows the same thermodynamic guidelines to minimize the free energy of the system. We postulate that the kinetics of assembly is the major determining factor in the distribution of final products when multiple reaction paths are thermodynamically possible. It may be the case that the products that dominate assembly are obtained via the fastest route with the shortest distance for linkers to traverse and the smallest energy barrier to overcome. It is also likely that the larger size of the origami tiles results in slower diffusion in solution, both laterally and rotationally, which affects the kinetics of the reaction. We stress that it is difficult to access the real-time dynamics of higher-order DNA self-assembly in solution because of the sophisticated nature of the tile–tile interactions, especially with the simultaneous association of multiple sticky ends. Nevertheless, analysis of the final products using AFM imaging still provides useful information about the assembly mechanism. As DNA origami tiles are gaining attention as potential building blocks for the bottom-up self-assembly of large superstructures, studies that reveal the influence of structural parameters such as dimensions, geometry, interunit connection strategies, and reaction conditions on assembly are imperative. Furthermore, by enhancing the rigidity of an origami tile to significantly increase the cost of bending or twisting the tile, we may be able to control the superstructure formation more reliably and avoid undesired reaction pathways. Our report highlights the need for the careful design of origami structures and assembly routes to achieve predictable products.

## Supplementary Material

Refer to Web version on PubMed Central for supplementary material.

## Acknowledgments

This work was partially supported by grants from the ONR, NSF, ARO, DOE, and NIH to Y.L. and H.Y. and from the Sloan Research Foundation to H.Y. Y.L. and H.Y. were supported by the Center for Bio-Inspired Solar Fuel Production, an Energy Frontier Research Center funded by the U.S. Department of Energy, Office of Science, Office of Basic Energy Sciences, under Award DE-SC0001016. This work was also supported by a scholarship to L.W. from the State Scholarship Fund of the China Scholarship Council. We thank Carol Flores for proofreading the manuscript.

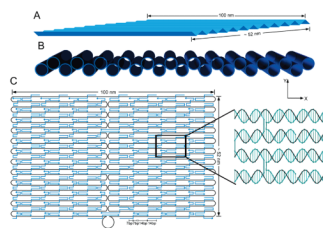
## References

1. Seeman NC. *Nature*. 2003; 421:427–431. [PubMed: 12540916]
2. Gothelf KV, LaBean TH. *Org Biomol Chem*. 2005; 3:4023–4037. [PubMed: 16267576]
3. Deng, Z.; Chen, Y.; Tian, Y.; Mao, C. *Nanotechnology: Science and Computation*. Chen, J.; Jonoska, N.; Rozenberg, G., editors. Springer; Berlin: 2006. p. 2334
4. Aldaye FA, Palmer A, Sleiman HF. *Science*. 2008; 321:1795–1799. [PubMed: 18818351]
5. Lin C, Liu Y, Yan H. *Biochemistry*. 2009; 48:1663–1674. [PubMed: 19199428]
6. Fu TJ, Seeman NC. *Biochemistry*. 1993; 32:3211–3220. [PubMed: 8461289]
7. Winfree E, Liu F, Wenzler LA, Seeman NC. *Nature*. 1998; 394:539–544. [PubMed: 9707114]
8. Mao C, Sun W, Seeman NC. *J Am Chem Soc*. 1999; 121:5437–5443.

9. LaBean TH, Yan H, Kopatsch J, Liu F, Winfree E, Reif JH, Seeman NC. *J Am Chem Soc.* 2000; 122:1848–1860.
10. Yan H, Park SH, Finkelstein G, Reif JH, LaBean TH. *Science.* 2003; 301:1882–1884. [PubMed: 14512621]
11. Liu D, Wang M, Deng Z, Walulu R, Mao C. *J Am Chem Soc.* 2004; 126:2324–2325. [PubMed: 14982434]
12. Ding B, Sha R, Seeman NC. *J Am Chem Soc.* 2004; 126:10230–10231. [PubMed: 15315420]
13. Rothmund PWK, Papadakis N, Winfree E. *PLoS Biol.* 2004; 2:2041–2053.
14. Chelyapov N, Brun Y, Gopalkrishnan M, Reishus D, Shaw B, Adleman L. *J Am Chem Soc.* 2004; 126:13924–13925. [PubMed: 15506744]
15. Rothmund P, Ekani-Nkodo A, Papadakis N, Kumar A, Fygenson D, Winfree E. *J Am Chem Soc.* 2004; 126:16344–16352. [PubMed: 15600335]
16. Mitchell JC, Harris JR, Malo J, Bath J, Turberfield AJ. *J Am Chem Soc.* 2004; 126:16342–14363. [PubMed: 15600334]
17. Malo J, Mitchell JC, Venien-Bryan C, Harris JR, Wille H, Sherratt DJ, Turberfield AJ. *Angew Chem, Int Ed.* 2005; 44:3057–3061.
18. Mathieu F, Liao S, Kopatsch J, Wang T, Mao C, Seeman NC. *Nano Lett.* 2005; 5:661–665. [PubMed: 15826105]
19. Park SH, Barish R, Li H, Reif JH, Finkelstein G, Yan H, LaBean TH. *Nano Lett.* 2005; 5:693–696. [PubMed: 15826110]
20. Ke Y, Liu Y, Zhang J, Yan H. *J Am Chem Soc.* 2006; 128:4414–4421. [PubMed: 16569019]
21. Chen J, Seeman NC. *Nature.* 1991; 350:631–633. [PubMed: 2017259]
22. Zhang Y, Seeman NC. *J Am Chem Soc.* 1994; 116:1661–1669.
23. Goodman RP, Berry RM, Turberfield AJ. *Chem Commun.* 2004; 1372–1373
24. Shih WM, Quispe JD, Joyce GF. *Nature.* 2004; 427:618–621. [PubMed: 14961116]
25. Goodman RP, Schaap IAT, Tardin CF, Erben CM, Berry RM, Schmidt CF, Turberfield AJ. *Science.* 2005; 310:1661–1665. [PubMed: 16339440]
26. He Y, Ye T, Su M, Zhang C, Ribbe AE, Jiang W, Mao C. *Nature.* 2008; 452:198–201. [PubMed: 18337818]
27. Zheng J, Birktoft JJ, Chen Y, Wang T, Sha R, Constantinou PE, Ginell SL, Mao C, Seeman NC. *Nature.* 2009; 461:74–77. [PubMed: 19727196]
28. Mirkin CA, Letsinger RL, Mucic RC, Storhoff JJ. *Nature.* 1996; 382:607–609. [PubMed: 8757129]
29. Alivisatos AP, Johnsson KP, Peng X, Wilson TE, Loweth CJ, Bruchez MP Jr, Schultz PG. *Nature.* 1996; 382:609–611. [PubMed: 8757130]
30. Le JD, Pinto Y, Seeman NC, Musier-Forsyth K, Taton TA, Kiehl RA. *Nano Lett.* 2004; 4:2343–2347.
31. Li H, Park SH, Reif JH, LaBean TH, Yan H. *J Am Chem Soc.* 2004; 126:418–419. [PubMed: 14719910]
32. Sharma J, Chhabra R, Liu Y, Ke Y, Yan H. *Angew Chem, Int Ed.* 2006; 45:730–735.
33. Zheng J, Constantinou PE, Micheel C, Alivisatos AP, Kiehl PA, Seeman NC. *Nano Lett.* 2006; 6:1502–1504. [PubMed: 16834438]
34. Chhabra R, Sharma J, Ke Y, Liu Y, Rinker S, Lindsay S, Yan H. *J Am Chem Soc.* 2007; 129:10304–10305. [PubMed: 17676841]
35. Sharma J, Chhabra R, Andersen CS, Gothelf KV, Yan H, Liu Y. *J Am Chem Soc.* 2008; 130:7820–7821. [PubMed: 18510317]
36. Rinker S, Ke Y, Liu Y, Chhabra R, Yan H. *Nat Nanotechnol.* 2008; 3:418–422. [PubMed: 18654566]
37. Sharma J, Chhabra R, Cheng A, Brownell J, Liu Y, Yan H. *Science.* 2009; 323:112–116. [PubMed: 19119229]
38. Bhatia D, Mehtab S, Krishnan R, Indi SS, Basu A, Krishnan Y. *Angew Chem, Int Ed.* 2009; 48:4134–4137.

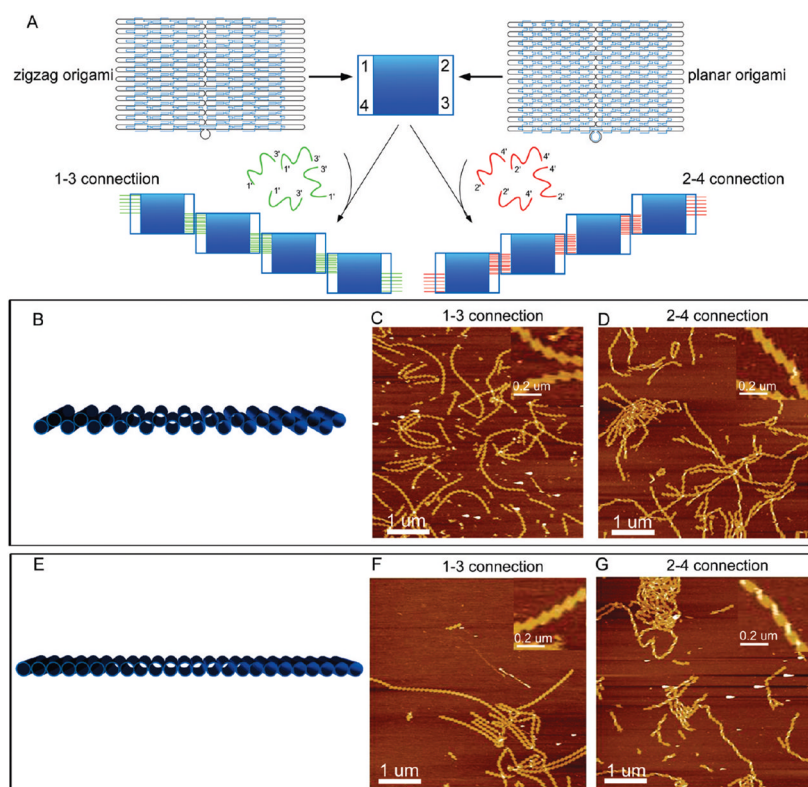


39. Mastroianni AJ, Claridge SA, Alivisatos AP. *J Am Chem Soc.* 2009; 131:8455–8459. [PubMed: 19331419]
40. Rothmund PWK. *Nature.* 2006; 440:297–302. [PubMed: 16541064]
41. Anderson ES, Dong M, Nielsen MM, Jahn K, Subramani R, Mamdouh W, Golas MM, Sander B, Stark H, Oliveira CLP, Pedersen JS, Birkedal V, Besenbacher F, Gothelf KV, Kjems J. *Nature.* 2009; 459:73–76. [PubMed: 19424153]
42. Douglas SM, Dietz H, Liedl T, Högberg B, Graf F, Shih WM. *Nature.* 2009; 459:414–418. [PubMed: 19458720]
43. Dietz H, Douglas SM, Shih WM. *Science.* 2009; 325:725–730. [PubMed: 19661424]
44. Pound E, Ashton JR, Becerril HA, Woolley AT. *Nano Lett.* 2009; 9:4302–4305. [PubMed: 19995086]
45. Kuzuya A, Komiyama M. *Chem Commun.* 2009; 4182–4184
46. Ke Y, Douglas SM, Liu M, Sharma J, Cheng A, Leung A, Liu Y, Shih WM, Yan H. *J Am Chem Soc.* 2009; 131:15903–15908. [PubMed: 19807088]
47. Zhao Z, Yan H, Liu Y. *Angew Chem, Int Ed.* 2010; 49:1414–1417.
48. Liedl T, Högberg B, Tytell J, Ingber DE, Shih WM. *Nat Nanotechnol.* 2010; 5:520–524. [PubMed: 20562873]
49. Ke Y, Lindsay S, Chang Y, Liu Y, Yan H. *Science.* 2008; 319:180–183. [PubMed: 18187649]
50. Shen W, Zhong H, Neff D, Norton ML. *J Am Chem Soc.* 2009; 131:6660–6661. [PubMed: 19400586]
51. Kuzyk A, Laitinen KT, Törmä P. *Nanotechnology.* 2009; 2:235305. [PubMed: 19448288]
52. Kuzuya A, Kimura M, Numajiri K, Koshi N, Ohnishi T, Okada F, Komiyama M. *ChemBioChem.* 2009; 10:1811–1815. [PubMed: 19562789]
53. Maune HT, Han S, Barish RD, Bockrath M, Goddard WA III, Rothmund PWK, Winfree E. *Nat Nanotechnol.* 2010; 5:61–66. [PubMed: 19898497]
54. Ding B, Deng Z, Yan H, Cabrini S, Zuckermann RN, Bokor J. *J Am Chem Soc.* 2010; 132:3248–3249. [PubMed: 20163139]
55. Pal S, Deng Z, Ding B, Yan H, Liu Y. *Angew Chem, Int Ed.* 2010; 49:2700–2704.
56. Voigt NV, Tørring T, Rotaru A, Jacobsen MF, Ravnsbæk JB, Subramani R, Mamdouh W, Kjems J, Mokhir A, Basen-bacher F, Gothelf KV. *Nat Nanotechnol.* 2010; 5:200–203. [PubMed: 20190747]
57. Lund K, Manzo AJ, Dabby N, Michelotti N, Johnson-Buck A, Nangreave J, Taylor S, Pei R, Stojanovic MN, Walter NG, Winfree E, Yan H. *Nature.* 2010; 465:206–210. [PubMed: 20463735]
58. Endo M, Sugita T, Katsuda Y, Hidaka K, Sugiyama H. *Chem –Eur J.* 2010; 16:5362–5368.
59. Sun X, Ko SH, Zhang C, Ribbe AE, Mao C. *J Am Chem Soc.* 2009; 131:13248–13249. [PubMed: 19715316]



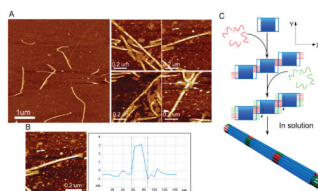
**Figure 1.**

Design of the zigzag DNA origami. (A) Schematic drawing of the rectangular-shaped corrugated tile having dimensions of 100 nm  $\times$  52 nm. (B) Side view of the tile illustrating the 120° dihedral angle formed between helices. (C) Folding path of the zigzag origami. A 7056 nt strand of M13mp18 (black) is folded into a rectangular structure using 168 staples (blue). The arrow on each staple strand indicates its 5' to 3' direction. The zoom-in view on the right shows structural details of selected staples.



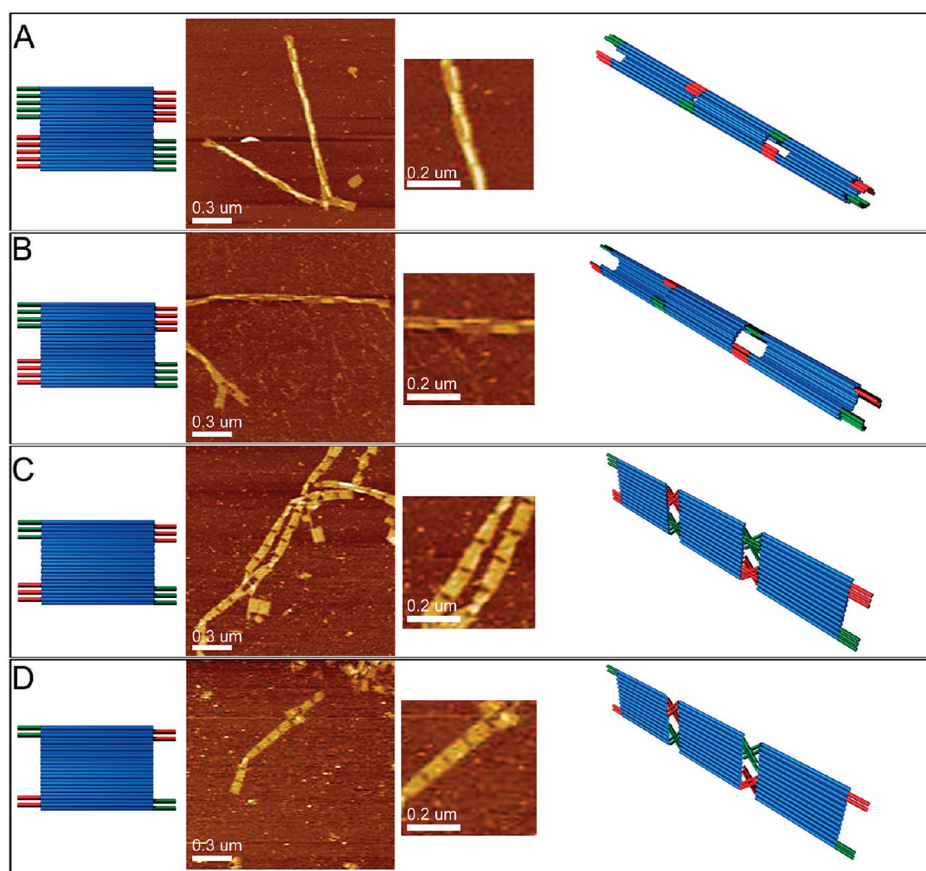
**Figure 2.**

Stairlike 1D DNA arrays assembled from the rectangular origami tiles. (A) For both designs, the core of each origami tile was assembled with the staple strands on the left and right edges omitted. The four corners involved in connecting individual origami tiles are numbered 1, 2, 3, and 4, each spanning 12 helices. Two sets of linker strands were designed, one to join corners 1 and 3 and the other corners 2 and 4. When all 12 linkers of the same set were added to the preannealed origami core structures, the cores were diagonally connected into stairlike ribbons. (B, E) Side views of the zigzag origami and planar origami, respectively. (C, F) AFM images of DNA ribbons formed by zigzag DNA origami and planar DNA origami, respectively, with 1–3 connections. Both tiles formed long ribbons, with the longest composed of ~40 tiles. (D, G) AFM images of DNA ribbons formed by zigzag DNA origami and planar DNA origami, respectively, with 2–4 connections. The zigzag origami formed long ribbons, similar to the case of 1–3 connections; the planar origami assembled into right-handed spiral ribbons, with every two or three tiles forming a half-turn twist. The insets in (C, D, F, and G) are zoom-in images.



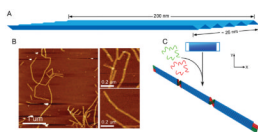
**Figure 3.**

DNA origami tubes. (A) AFM images of the tubular structure formed after the addition of both sets of linkers to the zigzag origami cores. Segments with lengths of 100 nm can be observed in the zoom-in images. (B) Cross-sectional profile of a tube measured along the thin white line in the image to the left of the profile: the height was 3 nm and the width ~30 nm. (C) Proposed mechanism for the formation of the origami tubes. Initially, one set of linkers binds to the complementary regions of neighboring core structures, creating a stairlike ribbon. Next, one binding domain in the other set of linkers binds to its complementary region of the core structure while the other binding domain subsequently binds to its complement in the adjacent tile. This interaction rolls the connected tiles into a tube whose axis is parallel to the origami helical axis and whose circumference equals the width of one tile.



**Figure 4.**

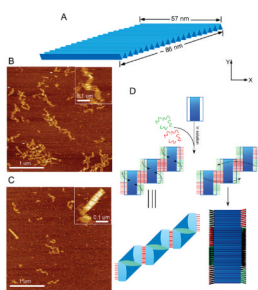
The number of linkers impacts the morphology of the resulting structures. (A, B) Use of 20 or 16 linkers results in the formation of tubes with broad circumferences. Shown in each panel from left to right are a schematic drawing of the number and position of linkers used for the connections between origami tiles, a zoom-out AFM image, a zoom-in AFM image, and a schematic drawing showing the assembled structure. (C, D) Use of 12 or 8 linkers results in the assembly of 1D chains.



**Figure 5.**

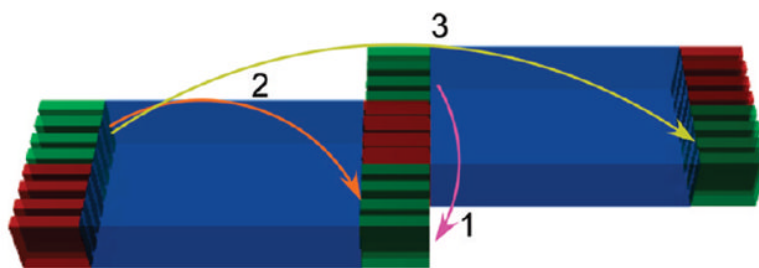
Formation of 1D chains by 12-helix zigzag origami tiles. (A) Schematic drawing of the 12-helix tile. (B) AFM images of the resulting 1D origami chains after the addition of 12 linker strands. Higher spots between two neighboring tiles can be clearly observed. (C) Hypothetical mechanism for the formation of 1D chains. The decreased width reduces the flexibility of the origami tiles significantly, so folding them in the  $y$  direction becomes unfavorable. Instead, the linkers prefer to cross in the center to connect origami tiles end-to-end into a chain. The overlapping linker strands form two-layer regions between neighboring tiles.








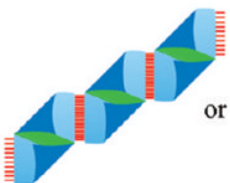





**Figure 6.**

Formation of zigzag ribbons or double-layered linear ribbons by 40-helix zigzag origami tiles. (A) Schematic drawing of the 40-helix origami tile. (B, C) AFM images of the resulting zigzag origami ribbons and double-layered linear ribbons, respectively. (D) Hypothetical mechanism for formation of these two structures. First, one set of linkers recognizes the complementary regions of the origami core, yielding staggered ribbons, after which the other set of linkers binds to complementary regions within the same tile or an adjacent tile. Binding to the same tile causes bulges within the staggered ribbons, giving a zigzag appearance, while binding to an adjacent tile results in linear, double-layered ribbons with growth in the y direction.



Origami tile	Linker number	Connection	Resulting structure
 100 nm X 52 nm	24	1	
	16 or 20	1	
	8 or 12	1	
 200 nm X 26 nm	12	1	
 57 nm X 86 nm	40	2 or 3	 or 

**Figure 7.**

Summary of the impact of varying the dimensional aspect ratio and intertile connection scheme of zigzag origami tile units on the resulting structures. The arrows labeled 1, 2, and 3 specify three different linking pathways.